Search for $e \to \tau$ Charged Lepton Flavor Violation at the EIC with the ECCE Detector

J.-L. Zhang[58], S. Mantry[69], J. K. Adkins[36], Y. Akiba[53,57], A. Albataineh[72], M. Amaryan[47], I. C. Arsene[76], C. Ayerbe Gayoso[38], J. Bae[62], X. Bai[81], M.D. Baker[4,28], M. Bashkanov[91], R. Bellwied[70], F. Benmokhtar[14], V. Berdnikov[12], J. C. Bernauer[55,56,57], F. Bock[49], W. Boeglin[16], M. Borysova[86], E. Brash[10], P. Brindza[28], W. J. Briscoe[20], M. Brooks[32], S. Bueltmann[47], M. H. S. Bukhari[27], A. Bylinkin[72], R. Capobianco[68], W.-C. Chang[2], Y. Cheon[60], K. Chen[7], K.-F. Chen[46], K.-Y. Cheng[40], M. Chiu[4], T. Chujo[79], Z. Citron[1], E. Cline[55,56], E. Cohen[44], T. Cormier[49], Y. Corrales Morales[32], C. Cotton[81], J. Crafts[12], C. Crawford[73], S. Creekmore[49], C.Cuevas[28], J. Cunningham[49], G. David[4], C. T. Dean[32], M. Demarteau[49], S. Diehl[68], N. Doshita[88], R. Dupré[23], J. M. Durham[32], R. Dzhygadlo[19], R. Ehlers[49], L. El Fassi[38], A. Emmert[81], R. Ent[28], C. Fanelli[37], R. Fatemi[73], S. Fegan[91], M. Finger[8], M. Finger Jr.[8], J. Frantz[48], M. Friedman[22], I. Friscic[37,28], D. Gangadharan[70], S. Gardner[18], K. Gates[18], F. Geurts[52], R. Gilman[54], D. Glazier[18], E. Glimos[49], Y. Goto[53,57], N. Grau[3], S. V. Greene[82], A. Q. Guo[25], L. Guo[16], S. K. Ha[89], J. Haggerty[4], T. Hayward[68], X. He[17], O. Hen[37], D. W. Higinbotham[28], M. Hoballah[23], T. Horn[12], A. Hoghmrtsyan[1], P.-h. J. Hsu[45], J. Huang[4], G. Huber[77], A. Hutson[70], K. Y. Hwang[90], C. E. Hyde[47], M. Inaba[66], T. Iwata[88], H.S. Jo[31], K. Joo[68], N. Kalantarians[84], G. Kalicy[12], K. Kawade[61], S. J. D. Kay[77], A. Kim[68], B. Kim[62], C. Kim[51], M. Kim[53], Y. Kim[51], Y. Kim[60], E. Kistenev[4], V. Klimenko[68], S. H. Ko[59], I. Korover[37], W. Korsch[73], G. Krintiras[72], S. Kuhn[47], C.-M. Kuo[40], T. Kutz[37], J. Lajoie[26], D. Lawrence[28], S. Lebedev[26], H. Lee[62], J. S. H. Lee[78], S. W. Lee[31], Y.-J. Lee[37], W. Li[52], W.B. Li[55,56,87], X. Li[64], X. Li[9], X. Li[32], X. Li[37], Y. T. Liang[25], S. Lim[51], C.-H. Lin[2], D. X. Lin[25], K. Liu[32], M. X. Liu[32], K. Livingston[18], N. Liyanage[81], W.J. Llope[85], C. Loizides[49], E. Long[75], R.-S. Lu[46], Z. Lu[9], W. Lynch[91], D. Marchand[23], M. Marcisovsky[13], C. Markert[1], P. Markowitz[16], H. Marukyan[1], P. McGaughey[32], M. Mihovilovic[74], R. G. Milner[37], A. Milov[86], Y. Miyachi[88], A. Mkrtchyan[1], P. Monaghan[10], R. Montgomery[18], D. Morrison[4], A. Movsisyan[1], H. Mkrtchyan[1], A. Mkrtchyan[1], C. Munoz Camacho[23], M. Murray[72], K. Nagai[32], J. Nagle[67], I. Nakagawa[53], C. Nattrass[80], D. Nguyen[28], S. Niccolai[23], R. Nouicer[4], G. Nukazuka[53], M. Nycz[81], V. A. Okorokov[43], S. Orešić[77], J.D. Osborn[49], C. O'Shaughnessy[32], S. Paganis[46], Z. Papandreou[77], S. F. Pate[42], M. Patel[26], C. Paus[37], G. Penman[18], M. G. Perdekamp[71], D. V. Perepelitsa[67], H. Periera da Costa[32], K. Peters[19], W. Phelps[10], E. Piasetzky[63], C. Pinkenburg[4], I. Prochazka[8], T. Protzman[34], M. L. Purschke[4], J. Putschke[85], J. R. Pybus[37], R. Rajput-Ghoshal[28], J. Rasson[49], B. Raue[16], K.F. Read[49], K. Røed[76], R. Reed[34], J. Reinhold[16], E. L. Renner[32], J. Richards[68], C. Riedl[71], T. Rinn[4], J. Roche[48], G. M. Roland[37], G. Ron[22], M. Rosati[26], C. Royon[72], J. Ryu[51], S. Salur[54], N. Santiesteban[37], R. Santos[68], M. Sarsour[17], J. Schambach[49], A. Schmidt[20], N. Schmidt[49], C. Schwarz[19], J. Schwiening[19], R. Seidl[53,57], A. Sickles[71], P. Simmerling[68], S. Sirca[74], D. Sharma[17], Z. Shi[32], T.-A. Shibata[41], C.-W. Shih[40], S. Shimizu[53], U. Shrestha[68], K. Slifer[75], K. Smith[32], D. Sokhan[18,24], R. Soltz[35], W. Sondheim[32], J. Song[9], J. Song[51], I. I. Strakovsky[20], P. Steinberg[4], P. Stepanov[12], J. Stevens[87], J. Strube[50], P. Sun[9], X. Sun[7], K. Suresh[77], V. Tadevosyan[1], W.-C. Tang[40], S. Tapia Araya[26], S. Tarafdar[82], L. Teodorescu[5], D. Thomas[1], A. Timmins[70], L. Tomasek[13], N. Trotta[68], R. Trotta[12], T. S. Tveter[76], E. Umaka[26], A. Usman[77], H. W. van Hecke[32], C. Van Hulse[23], J. Velkovska[82], E. Voutier[23], P.K. Wang[23], Q. Wang[72], Y. Wang[7], Y. Wang[65], D. P. Watts[91], N. Wickramaarachchi[12], L. Weinstein[47], M. Williams[37], C.-P. Wong[32], L. Wood[50], M. H. Wood[6], C. Woody[4], B. Wyslouch[37], Z. Xiao[65], Y. Yamazaki[30], Y. Yang[39], Z. Ye[65], H. D. Yoo[90], M. Yurov[32], N. Zachariou[91], W.A. Zajc[11], W. Zha[64], J.-X. Zhang[81], Y. Zhang[65], Y.-X. Zhao[25], X. Zheng[81], P. Zhuang[65]

[1]*A. Alikhanyan National Laboratory, Yerevan, Armenia*
[2]*Institute of Physics, Academia Sinica, Taipei, Taiwan*
[3]*Augustana University, Sioux Falls, SD, USA*
[4]*Brookhaven National Laboratory, Upton, NY, USA*
[5]*Brunel University London, Uxbridge, UK*
[6]*Canisius College, Buffalo, NY, USA*
[7]*Central China Normal University, Wuhan, China*
[8]*Charles University, Prague, Czech Republic*
[9]*China Institute of Atomic Energy, Fangshan, Beijing, China*
[10]*Christopher Newport University, Newport News, VA, USA*
[11]*Columbia University, New York, NY, USA*
[12]*Catholic University of America, Washington DC, USA*
[13]*Czech Technical University, Prague, Czech Republic*
[14]*Duquesne University, Pittsburgh, PA, USA*
[15]*Duke University, Durham NC, USA*
[16]*Florida International University, Miami, FL, USA*
[17]*Georgia State University, Atlanta, GA, USA*
[18]*University of Glasgow, Glasgow, UK*
[19]*GSI Helmholtzzentrum fuer Schwerionenforschung GmbH, Darmstadt, Germany*
[20]*The George Washington University, Washington, DC, USA*

[21]*Hampton University, Hampton, VA, USA*
[22]*Hebrew University, Jerusalem, Isreal*
[23]*Universite Paris-Saclay, CNRS/IN2P3, IJCLab, Orsay, France*
[24]*IRFU, CEA, Universite Paris-Saclay, Gif-sur-Yvette France*
[25]*Chinese Academy of Sciences, Lanzhou, China*
[26]*Iowa State University, Iowa City, IA, USA*
[27]*Jazan University, Jazan, Sadui Arabia*
[28]*Thomas Jefferson National Accelerator Facility, Newport News, VA, USA*
[29]*James Madison University, Harrisonburg, VA, USA*
[30]*Kobe University, Kobe, Japan*
[31]*Kyungpook National University, Daegu, Republic of Korea*
[32]*Los Alamos National Laboratory, Los Alamos, NM, USA*
[33]*Lawrence Berkeley National Lab, Berkeley, CA, USA*
[34]*Lehigh University, Bethlehem, PA, USA*
[35]*Lawrence Livermore National Laboratory, Livermore, CA, USA*
[36]*Morehead State University, Morehead, KY,*
[37]*Massachusetts Institute of Technology, Cambridge, MA, USA*
[38]*Mississippi State University, Mississippi State, MS, USA*
[39]*National Cheng Kung University, Tainan, Taiwan*
[40]*National Central University, Chungli, Taiwan*
[41]*Nihon University, Tokyo, Japan*
[42]*New Mexico State University, Las Cruces, NM, USA*
[43]*National Research Nuclear University MEPhI, Moscow, Russian Federation*
[44]*Nuclear Research Center - Negev, Beer-Sheva, Isreal*
[45]*National Tsing Hua University, Hsinchu, Taiwan*
[46]*National Taiwan University, Taipei, Taiwan*
[47]*Old Dominion University, Norfolk, VA, USA*
[48]*Ohio University, Athens, OH, USA*
[49]*Oak Ridge National Laboratory, Oak Ridge, TN, USA*
[50]*Pacific Northwest National Laboratory, Richland, WA, USA*
[51]*Pusan National University, Busan, Republic of Korea*
[52]*Rice University, Houston, TX, USA*
[53]*RIKEN Nishina Center, Wako, Saitama, Japan*
[54]*The State University of New Jersey, Piscataway, NJ, USA*
[55]*Center for Frontiers in Nuclear Science, Stony Brook, NY, USA*
[56]*Stony Brook University, Stony Brook, NY, USA*
[57]*RIKEN BNL Research Center, Upton, NY, USA*
[58]*Shandong University Qingdao, Shandong, China*
[59]*Seoul National University, Seoul, Republic of Korea*
[60]*Sejong University, Seoul, Republic of Korea*
[61]*Shinshu University, Matsumoto, Nagano, Japan*
[62]*Sungkyunkwan University, Suwon, Republic of Korea*
[63]*Tel Aviv University, Tel Aviv, Israel*
[64]*University of Science and Technology of China, Hefei, China*
[65]*Tsinghua University, Beijing, China*
[66]*Tsukuba University of Technology, Tsukuba, Ibaraki, Japan*
[67]*University of Colorado Boulder, Boulder, CO, USA*
[68]*University of Connecticut, Storrs, CT, USA*
[69]*University of North Georgia, Dahlonega GA, USA*
[70]*University of Houston, Houston, TX, USA*
[71]*University of Illinois, Urbana, IL, USA*
[72]*Unviersity of Kansas, Lawrence, KS, USA*
[73]*University of Kentucky, Lexington, KY, USA*
[74]*University of Ljubljana, Ljubljana, Slovenia, Ljubljana, Slovenia*
[75]*University of New Hampshire, Durham, NH, USA*
[76]*University of Oslo, Oslo, Norway*
[77] *University of Regina, Regina, SK, Canada*
[78]*University of Seoul, Seoul, Republic of Korea*
[79]*University of Tsukuba, Tsukuba, Japan*
[80]*University of Tennessee, Knoxville, TN, USA*
[81]*University of Virginia, Charlottesville, VA, USA*
[82]*Vanderbilt University, Nashville, TN, USA*
[83]*Virginia Tech, Blacksburg, VA, USA*
[84]*Virginia Union University, Richmond, VA, USA*
[85]*Wayne State University, Detroit, MI, USA*
[86]*Weizmann Institute of Science, Rehovot, Israel*
[87]*The College of William and Mary, Williamsburg, VA, USA*
[88]*Yamagata University, Yamagata, Japan*
[89]*Yarmouk University, Irbid, Jordan*
[90]*Yonsei University, Seoul, Republic of Korea*
[91]*University of York, York, UK*

[92]University of Zagreb, Zagreb, Croatia

Abstract

The recently approved Electron-Ion Collider (EIC) will provide a unique new opportunity for searches of charged lepton flavor violation (CLFV) and other new physics scenarios. In contrast to the $e \leftrightarrow \mu$ CLFV transition for which very stringent limits exist, there is still a relatively large discovery space for the $e \to \tau$ CLFV transition, potentially to be explored by the EIC. With the latest detector design of ECCE (EIC Comprehensive Chromodynamics Experiment) and projected integral luminosity of the EIC, we find the τ-leptons created in the DIS process $ep \to \tau X$ are expected to be identified with high efficiency. A first ECCE simulation study, restricted to the 3-prong τ-decay mode and with limited statistics for the Standard Model backgrounds, estimates that the EIC will be able to improve the current exclusion limit on $e \to \tau$ CLFV by an order of magnitude.

1. Charged-Lepton Flavor Violation and Leptoquarks

The discovery of neutrino oscillations provided conclusive evidence of lepton flavor violation. Lepton flavor violation in the neutrino sector also results in charged lepton flavor violation (CLFV) through loop-suppressed processes such as $\mu \to e\gamma$. However, the resulting predicted CLFV rates are highly suppressed due to the small neutrino masses – $\mathrm{Br}(\mu \to e\gamma) < 10^{-54}$ – and are far beyond the reach of any current or planned experiments. On the other hand, many Beyond Standard Models (BSM) scenarios predict CLFV rates that are both much larger and within reach of ongoing or near-future experiments. For example, supersymmetry-based models predict rates as high as $\mathrm{Br}(\mu \to e\gamma) \sim 10^{-15}$ [1], while the current experimental limit on the $\mu \to e\gamma$ process already reached $\mathrm{Br}(\mu \to e\gamma) < 4.2 \times 10^{-13}$ [2]. On the other hand, while there have been extensive searches for CLFV processes between the first and second lepton generations, denoted as CLFV(1,2) for brevity, the constraints on CLFV(1,3) processes that involve $e \leftrightarrow \tau$ transitions are weaker by several orders of magnitude. These constraints on CLFV(1,3) [3, 4] were obtained through searches for $e + p \to \tau + X$, $\tau \to e\gamma$, and $p+p \to e+\tau+X$ at HERA [5, 6], BaBar [7], and the LHC [8] respectively. However, there are many BSM scenarios such as grand unified theories with leptoquarks and R-parity violating supersymmetry that predict CLFV(1,3) rates that are enhanced compared to CLFV(1,2) processes, motivating continued searches dedicated for $e \leftrightarrow \tau$ transitions.

We carry out the simulation analysis based on the design of the ECCE Detector (recommended as Detector 1 by the EIC Detector Proposal Advisory Panel [9]), for determining the sensitivity to the CLFV(1,3) process $e+p \to \tau+X$ in the leptoquark framework [3, 4], though such analysis could also be performed in the SMEFT framework [4]. Leptoquarks are color triplet bosons that carry both lepton (L) and baryon (B) numbers, coupling leptons to quarks and mediating the $e + p \to \tau + X$ CLFV(1,3) process at tree-level, as shown in Fig. 1. The leptoquarks are classified into 14 types [10] based on their fermion number $F = 3B + L$ ($F = 0$ or $|F| = 2$), spin (scalar or vector), chiral couplings to leptons (left-handed or right-randed), $SU(2)_L$ representation (singlet, doublet, or triplet), and $U(1)_Y$ hypercharge.

In the region where the leptoquark mass M_{LQ} is much larger than the characteristic energy scale of the experiment, represented by the center-of-mass energy $\sqrt{s}$ and the four-momentum transfer $\sqrt{Q^2}$, the CLFV(1,3) process $e + p \to \tau + X$ is mediated by a contact interaction and the tree-level cross section for $F = 0$ or $|F| = 2$ leptoquarks takes the form:

$$
\begin{aligned}
\sigma_{F=0} &= \sum_{\alpha,\beta} \frac{s}{32\pi}\left[\frac{\lambda_{1\alpha}\lambda_{3\beta}}{M_{LQ}^2}\right]^2 \times \\
&\int dx \int dy \,\{x\bar{q}_\alpha(x, xs) f(y) + x q_\beta(x, -u) g(y)\}, \\
\sigma_{|F|=2} &= \sum_{\alpha,\beta} \frac{s}{32\pi}\left[\frac{\lambda_{1\alpha}\lambda_{3\beta}}{M_{LQ}^2}\right]^2 \times \\
&\int dx \int dy \,\{x q_\alpha(x, xs) f(y) + \bar{q}_\beta(x, -u) g(y)\},
\end{aligned} \quad (1)
$$

where $u = x(y-1)s$ with x the Bjorken scaling variable and y the fractional energy loss of the electron in the proton-rest frame. The kinematic y-dependent functions $f(y), g(y)$ are $f(y) = 1/2, g(y) = (1-y)^2/2$ and $f(y) = 2(1-y)^2, g(y) = 2$ for scalar and vector leptoquarks, respectively. The quantity $\lambda_{1\alpha}\lambda_{3\beta}/(M_{LQ}^2)$ characterizes the strength of the contact interaction. The λ_{ij} parameters, assumed to be real numbers for this analysis, denote the leptoquark couplings between the i-th lepton generation and j-th quark generation.

The ZEUS and H1 experiments at HERA placed upper limits on $\lambda_{1\alpha}\lambda_{3\beta}/M_{LQ}^2$ [11, 5, 12, 6]. The HERA data set corresponded to $\sqrt{s} = 300$ and 318 GeV and a total integrated luminosity of up to 130 pb^{-1}. With several orders of magnitude increase in the luminosity, the EIC has the potential to improve upon the HERA limits for both diagonal ($\alpha = \beta$) and off-diagonal ($\alpha \neq \beta$) components, and provide complementary information [4] to the constraints

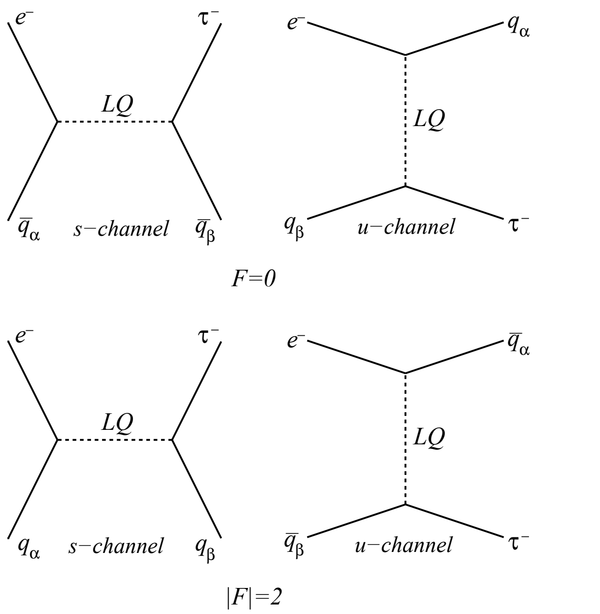

Figure 1: From [3]: Representative Feynman diagrams for $e \rightarrow \tau$ scattering processes via one-leptoquark mediator. The fermionic number F is assumed to be conserved, as in the BRW effective model [10]. The partonic cross section is convoluted with the PDF of the initial state (anti)quark of each diagram, and depends on the parameter $\lambda_{1\alpha}\lambda_{3\beta}/M_{LQ}^2$.

from BaBar and the LHC.

2. EIC/ECCE Simulation and Vertex Identification

The EIC Comprehensive Chromodynamics Experiment (ECCE) detector concept [13] addresses the full EIC science mission as described in the EIC community White Paper [14] and the 2018 National Academies of Science (NAS) Report [15]. It is simultaneously fully capable, low-risk, and cost-effective. ECCE strategically repurposes select components of existing experimental equipment to maximize its overall capabilities within the envelope of planned resources. For example, the central barrel of the detector incorporates the storied 1.4 T BaBar superconducting solenoid, and the sPHENIX barrel hadronic calorimeter currently under construction.

The goal of this work is to study the potential for discovering the $e^-p \rightarrow \tau^-X$ CLFV process at the EIC based on realistic detector simulations, and identification of such events over Standard Model (SM) backgrounds that include neutral-current (NC) deep inelastic scattering (DIS), charged-current (CC) DIS, and photoproductions. CLFV events leading to a final-state τ and are characterized by a high-momentum isolated τ which is balanced by a jet in the transverse plane. Since the τ will decay into stable particles after a short flying distance of $\sim \mu$m, only its decay products are visible in the detector. A critical requirement of CLFV searches is thus the secondary vertex reconstruction performance which relies on the tracking and especially the vertex detectors. The ECCE conceptual design uses state-of-the-art technologies consisting Monolithic Active Pixel Sensor (MAPS) based silicon vertex/tracking subsystem to achieve high precision primary and decay vertex determination.

The three SM background processes affect the CLFV searches as follows: First, the SM NC DIS events are very similar to leptoquark events where the τ decays to only one charged particle plus neutrinos in the final state, making this channel very difficult to study. Secondly, due to the presence of at least one neutrino in all τ-decay channels, significant missing p_T is expected. This feature is similar to the SM CC DIS events. The third main background of concern is from photoproduction events, mostly due to their very high yield. In this study, we focus the identification of CLFV candidate events that contain a high-p$_T$ quark-initiated jet along with an isolated and high-p$_T$ τ which replaces the scattered electrons in the typical NC DIS events, and the rejection of events from all three SM background processes.

Based on the number of the charged particles in the final state, the dominant τ decay modes can be categorized into "1-prong" (one charged particle) and "3-prong" (three charged particles). The "3-prong" decay modes have a branching ratio of ~15% while the "1-prong" modes have a branching ratio of ~85%. Although the "1-prong" modes have larger branching ratio, they are more demanding to identify. For example, the "1-prong" mode could be one of the two leptonic decays, $\tau \rightarrow e\bar{\nu}_e\nu_\tau$ or $\tau \rightarrow \mu\bar{\nu}_\mu\nu_\tau$. If the charged particle is an electron, it is very similar to DIS NC events. If the charged particle is a muon, it will require good muon identification. Another possible "1-prong" mode is $\tau \rightarrow \nu_\tau\pi^-$, containing one charged pion, and can be studied in the near future. In this study, we focus only on searching for the τ "3-prong" decay events.

The features of "3-prong" leptoquark events include: 1) no scattered electron is detected; 2) a high transverse-momentum (P_T) τ-jet consists of three charged particles within a relatively small cone; 3) all three charged particles originate from a common secondary vertex; 4) a high P_T hadronic jet is found back-to-back from the τ-jet; and 5) a P_T-imbalance caused by the escaped neutrinos which should be part of the candidate τ-jet. In order to simulate such candidate events and the capability to identify them, the leptoquark quark generator LQGENEP [16] (version 1.0) is used to produce the signal Monte-Carlo (MC) events, while Djangoh and Pythia generators are used to produce the background DIS and photoproduction MC events, respectively. Considering the large mass of leptoquarks, we focus on the highest energy, 18×275 GeV ep collision. For the LQGENEP simulation, the Q^2 range is set to > 10 GeV^2 and a default value of leptoquark mass 1.9 TeV from the generator is used, see Appendix A.1 for input files. Scanning through a series of leptoquark mass values, no visible difference in the characteristics of these signal events was observed at EIC kinematics. The input files for background event generation are given in Appendix A.2 for DIS NC and CC, and Appendix A.3

for photoproduction. After passing the generated events through the ECCE GEANT4 simulation, an analysis algorithm with preliminary selection requirements based on the features of the signal and background events are applied on both leptoquark and SM MC event samples.

As mentioned earlier, a precise identification capability of the interaction vertex is essential for the secondary vertex reconstruction and τ identification. Figure 2 shows the vertex resolution for different track multiplicities, where we see that the ECCE configuration can provide a vertex resolution of $20-30\mu$m while the decay length of τ lepton is $\sim 87\mu$m. Therefore the ECCE vertex resolution is sufficient for identifying τ decays.

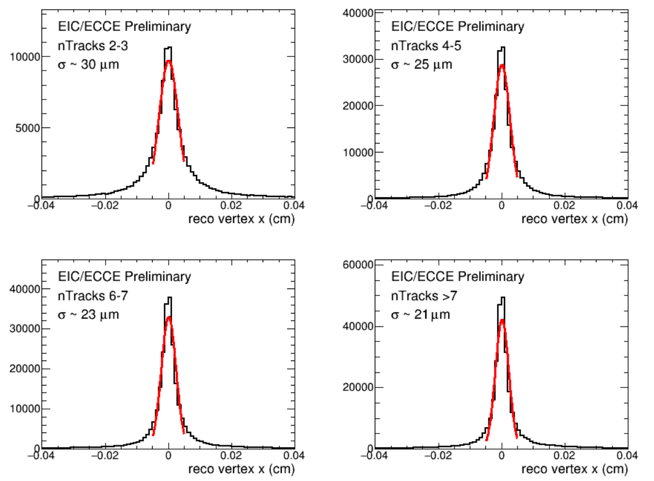

Figure 2: Primary vertex resolution: difference between truth and reconstructed information for different track multiplicity. Only the x-component is shown here, while y- and z-components show similar characteristics but are not shown.

To reconstruct the secondary vertex, we first look for 3-π candidate events. In the following, the charged pion's tracking information is from the simulated tracking and the vertex detector responses, though particle identification (PID) is based on generator information (namely, perfect PID is assumed). In our algorithm, one track is matched to a second track and the middle point at the closest approach is the candidate secondary vertex position which will be further justified based on the topological structure. For a given 3-π candidate event, there are three such pair-combinations and we can reconstruct three "intermediate" vertices and the candidate vertex will be the average of all three. Figure 3 shows the correlation of three intermediate vertices from the three pair combinations where the three decay lengths dl_{12}, dl_{13}, and dl_{23}, as extracted by the distance from the primary to the secondary "intermediate" vertices, are shown as the x-axis, the positive half of the y-axis, and the negative half of the y-axis, respectively. There are clearly two bands centralized at lines $y = \pm x$ and the 3-π vertex can be identified by requiring either or both correlations. In fact, when combined with vector alignment cuts, coincidence between two of the three "intermediate" vertices (either upper or lower half of Fig. 3) is usually enough to indicate a "3-prong" secondary vertex.

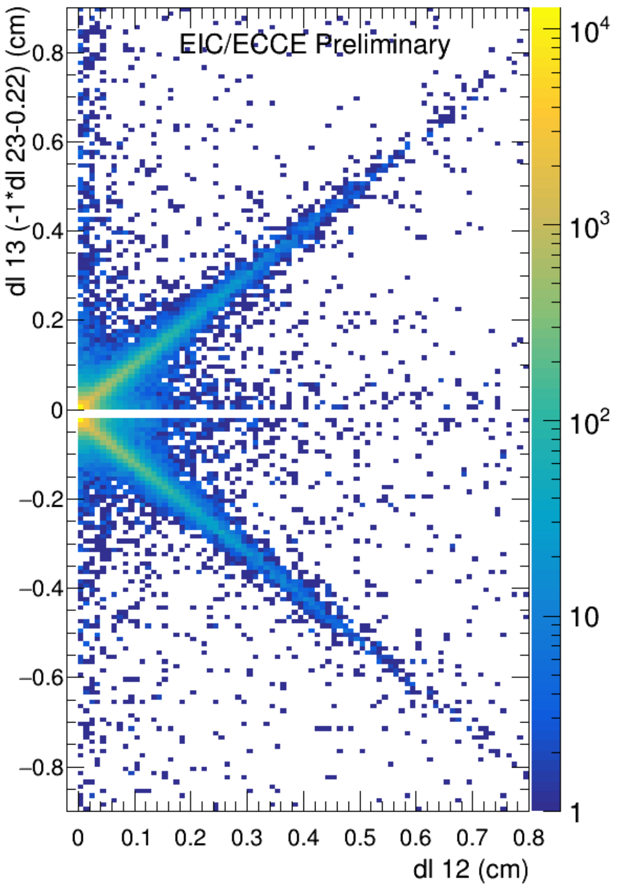

Figure 3: Coincidence among three "intermediate" vertices for 3-π event identification. The x-axis, the positive y and the negative y-axis (displaced and direction reversed for clarity), represent the "intermediate" vertices from the three pair-combinations 12, 13 and 23, respectively.

3. Event Selection

We used ten selection criteria to identify $e \to \tau$ events and to reject SM backgrounds. Their effects are shown in Fig. 4, where the vertical axis shows how many sample events pass each of the selection criteria, and the horizontal axis are the progressive selections defined as follows:

- input: initial input events. We used 10^6 (1M) MC events for each of leptoquark, DIS NC, DIS CC, and photoproduction processes;
- PrVtx: there must be a primary vertex reconstructed;
- Epzh: $\sum_h (E - p_z) > 18$ GeV, where E and p_z are the energy and the z–component (along the beams) of the 3-momentum of the final state particles, respectively, and the summation is over all detected hadrons;
- misspt: $1 <$ missing $p_T < 9$ GeV, here the lower limit is to suppress events with small missing p_T, e.g. photoproduction events, and the upper limit is to suppress

DIS events with large missing p_T caused by neutrinos (CC) or miss-detected electrons (NC);

- 3-pion: candidate 3 charged pions are found in a $\Delta R < 1.0$ cone, where R is cone radius in the azimuth(ϕ)-pseudorapidity(η) space, $\Delta R \equiv \sqrt{\Delta\phi^2 + \Delta\eta^2}$;
- away1GeV: p_T sum of all tracks on the away-side of the candidate 3-π, $\sum_{\Delta\phi(-\vec{p}_{3\pi})<1.0} p_T$, is > 1 GeV;
- nearIso: p_T sum in a cone around the candidate 3-π, $\sum_{\Delta R(\vec{p}_{3\pi})<1.0} p_T$, is < 3.0 GeV;
- 3pi_pt: p_T sum of the 3 charged-pion candidate, $p_{T(3\pi)}$, is > 3.0 GeV;
- 30μm: candidate decay length reconstructed from any pair of the 3 charged pions is > 30μm;
- dRsum: sum of the "distances" (in $\phi - \eta$ space) of the 3 charged pions decay vectors, $\Delta R_{1,2} + \Delta R_{1,3} + \Delta R_{2,3}$, is < 0.4. Here the decay vector is defined as starting from the primary vertex and pointing to the secondary vertex;
- decayL: average of the reconstructed decay lengths from three pair combinations of the 3-π candidate, $(dl_{12} + dl_{13} + dl_{23})/3$, is > 0.5 mm;
- cMass: $\sqrt{M_{3\pi}^2 + p_{3\pi}^2 \sin^2\theta} + p_{3\pi}\sin^2\theta < 1.8$ GeV, where θ is the angle between the reconstructed decay direction and the 3π momentum direction, and $M_{3\pi}$ is the mass reconstructed from the 3-π [17];
- missing phi: missing p_T is azimuthally on the near side of the candidate 3-π, that is, $\Delta\phi$ between $\vec{p_{3\pi}}$ and $\vec{p_T^{miss}}$ is < 1.0.

From Fig. 4, it can be seen that the $e \to \tau$ events can be effectively selected with this set of preliminary cuts. In addition, selections using the decay length are the most discriminating feature of the τ-jet. We illustrate this feature, characterized by the precision of ECCE's vertex detector, in Fig. 5. The left panel shows a comparison between the true decay length from the generator and the decay length reconstructed from tracks at the detector level, while the right panel shows a 119 μm resolution of the decay length under ECCE configuration, capable for the τ vertex identification.

4. Sensitivity to Leptoquarks

We can now deduce the sensitivity to the leptoquark signal cross section based on simulations of the 3-prong decay mode (15% branching ratio) of the τ lepton, discussed in the last section, and considering different possible values for the detection efficiency of the other τ decay modes. In Fig. 4, 1M MC event samples are generated for each of the four processes: the leptoquark mediated signal process $e + p \to \tau + X$, and three background processes, NC DIS, CC DIS, and photoproduction. After all selection cuts are applied, including the requirement of detecting three pions corresponding to the 3-prong tau decay mode, about 8K (7878) of the original 1M leptoquark signal events remain. For an integrated luminosity of 100 fb $^{-1}$, the 1M signal events generated corresponds to a signal cross section of 10^4fb. Thus, if we assume that only the 3-prong mode has a non-zero detection efficiency, the minimum required cross section for detecting a single signal event in the 3-prong mode is 10^4 fb/7878 = 1.3 fb. On the other hand, if we allow for the other tau decay modes and assume that they can be detected with the same efficiency as the 3-prong decay mode, then the number of candidate events that now survive selection cuts will be 7878/(15%) = 52520. Thus, in this case the minimum required cross section for detecting a single signal event will be 10^4fb/52520 = 0.19 fb. We also consider an intermediate scenario in which, in addition to the 3-prong mode, we allow for the muon and single charge pion decay modes (~ 40 % branching ratio) and assume they can be detected at half the detection efficiency of the 3-prong decay. In this case the total number of candidate events that now survive all selection cuts will be 7878+7878/(15%)×(40%)×1/2 = 18382. In this case, the minimum required cross section to detect a single signal event is 10^4fb/18382 = 0.54 fb.

For searches of rare events like leptoquark mediated $e \to \tau$ transitions, the background simulation is more difficult than the signal. Among the three types of background events, the CC DIS background is easier to estimate because the total cross section is only $\approx 2.3 \times 10^4$ fb, and the 1 M CC DIS MC events generated correspond to about 43% of the expected statistics for 100 fb^{-1} of integrated luminosity. There are 4 CC DIS events that pass the event selection, which can be scaled up to 4/43% = 9 events for 100 fb^{-1}. With more careful optimization, this number can be suppressed even further. On the other hand, the NC DIS and photoproduction backgrounds are much harder to evaluate because their cross sections are much larger and of order 10^7 fb. Thus, the 1M generated MC events correspond to only $\sim 10^6/(10^7\text{fb} \times 100\text{fb}^{-1}) =$ 0.1% of the expected data sample for 100 fb^{-1} of integrated luminosity. With this limited MC event sample, zero NC and photoproduction event satisfies all selection criteria. Thus, at this stage, it is difficult to estimate how many background events will survive the selection if the MC sample is increased by factor 10^3, which is needed to simulate 100 fb^{-1} of NC DIS and photoproduction data.

At the moment, instead of providing a specific estimate of the background, we show in Fig. 6 the leptoquark cross-section ECCE could be sensitive to as a function of the number of background events that survive the event selection for 100 fb^{-1} of integrated luminosity, based on a simple calculation as follows: If the number of background events is B, the number of leptoquark signal events S should exceed the "3σ" limit of the expected observed background events, $S + B > B + 3\sqrt{B}$, for the signal to be established. The corresponding cross section is scaled from the value where only one leptoquark signal event can be observed ($S = 1$).

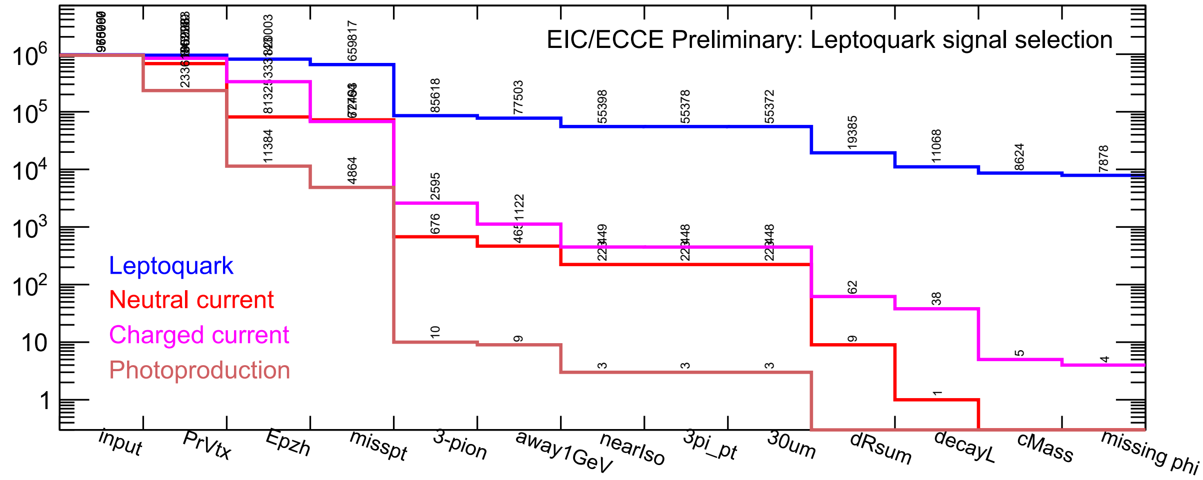

Figure 4: MC statistics of leptoquark (blue), DIS CC (red), DIS NC (magenta), and photoproduction (orange) events, as ten selection criteria are progressively applied on 1 M input events for each channel. Please see text for details.

As a best-case scenario estimate of the sensitivity to the leptoquark signal cross section, we do not consider any NC and photoproduction background event since none of these events passed all the selection cuts on our limited MC event sample. For a 5σ (99.99994% confidence level) discovery criteria of $S/\sqrt{(B)} \geq 5$ (S being signal and B being background) and use $B = 9$ events from CC background, we need $S = 15$ leptoquark events or a total of $15 + 9 = 24$ events to claim $e \to \tau$ CLFV discovery. Alternatively, detection of less than $9 + 9 = 18$ events will provide a 3σ (99.7% C.L.) exclusion limit on the leptoquark cross section, which would be 1.3 fb$\times 3\sqrt{9}$ = 11.4 fb, 0.54 fb$\times 3\sqrt{9}$ = 5.0 fb, and 0.19 fb$\times 3\sqrt{9}$ = 1.7 fb, for detection possibility of "3-prong only", "3-prong + 1-prong with 50% efficiency", and "all decay modes detected with same efficiency as 3-prong", respectively. The exclusion potential, expressed in terms of $\lambda_{1\alpha}\lambda_{3\beta}/M_{LQ}^2$, are shown in Figs. 7 and 8 for scalar and vector leptoquark states, respectively. This is a preliminary estimate, and different statistical methods and a larger MC event sample to better estimate NC DIS and photoproduction backgrounds could give rise to different estimates.

5. Summary

We carried out the first projection analysis for charged lepton flavor violation in the $e \to \tau$ transition channel, using EIC simulations with the ECCE detector configuration. More work needs to be done in the future alongside the development of ECCE into a project detector, such as using detector-based particle identification, study more τ decay modes, and carry out the background study with higher statisitics. Our current study, using the simulation and detector resources at hand, shows that the EIC will place a more stringent limit on $e \to \tau$ CLFV mediated by leptoquarks than the previous HERA data. The very high vertex resolution of the ECCE detector configuration plays a critical role in our study.

6. Acknowledgements

We thank the EIC Silicon Consortium for cost estimate methodologies concerning silicon tracking systems, technical discussions, and comments. We acknowledge the important prior work of projects eRD16, eRD18, and eRD25 concerning research and development of MAPS silicon tracking technologies.

We thank the EIC LGAD Consortium for technical discussions and acknowledge the prior work of project eRD112.

We thank Guillelmo Gomez Ceballos Retuerto and Hubert Spiesberger for their useful discussions and comments.

We acknowledge support from the Office of Nuclear Physics in the Office of Science in the Department of Energy, the National Science Foundation, and the Los Alamos National Laboratory Laboratory Directed Research and Development (LDRD) 20200022DR.

References

[1] R. Barbieri, L. J. Hall, A. Strumia, Violations of lepton flavor and CP in supersymmetric unified theories, Nucl. Phys. B 445 (1995) 219–251. `arXiv:hep-ph/9501334`, `doi:10.1016/0550-3213(95)00208-A`.

[2] A. M. Baldini, et al., Search for the lepton flavour violating decay $\mu^+ \to e^+\gamma$ with the full dataset of the MEG experiment, Eur. Phys. J. C 76 (8) (2016) 434. `arXiv:1605.05081`, `doi:10.1140/epjc/s10052-016-4271-x`.

[3] M. Gonderinger, M. J. Ramsey-Musolf, Electron-to-Tau Lepton Flavor Violation at the Electron-Ion Collider, JHEP 11 (2010) 045, [Erratum: JHEP 05, 047 (2012)]. `arXiv:1006.5063`, `doi:10.1007/JHEP11(2010)045`.

[4] V. Cirigliano, K. Fuyuto, C. Lee, E. Mereghetti, B. Yan, Charged Lepton Flavor Violation at the EIC, JHEP 03 (2021) 256. `arXiv:2102.06176`, `doi:10.1007/JHEP03(2021)256`.

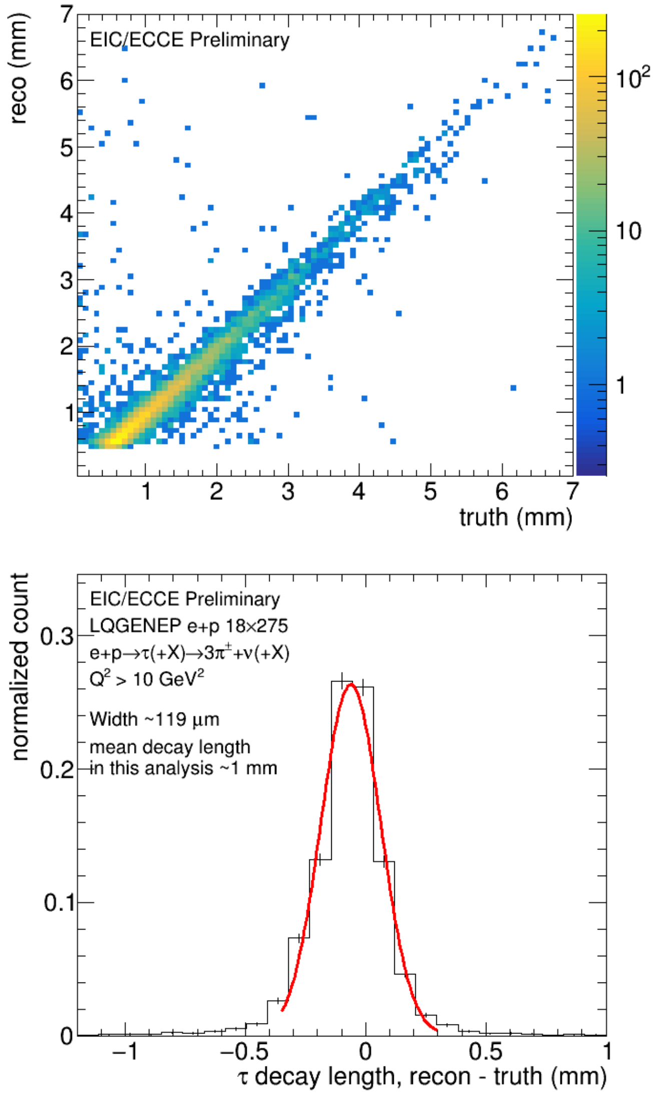

Figure 5: Top: Reconstructed decay length from Geant4 detector simulation vs. true decay length from generator level. Bottom: difference between reconstructed and true decay length with a Gaussian fit.

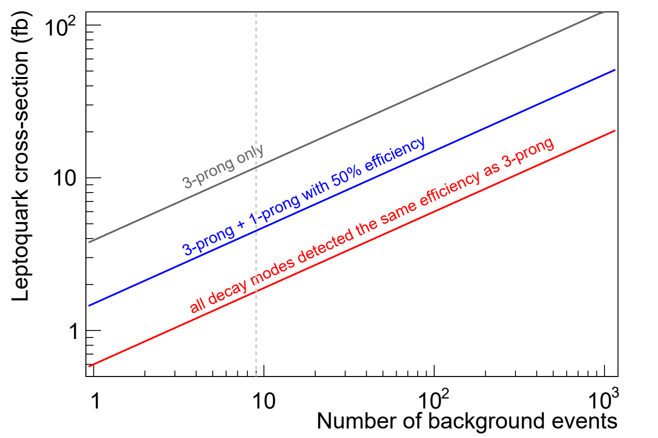

Figure 6: Cross section sensitivity for leptoquark search vs number of residual background events for 100 fb^{-1} integrated luminosity. The grey line corresponds to the scenario that only "3-prong" decay modes are detected. The blue line corresponds to the scenario where electron and pion "1-prong" decay modes could be detected with 50% efficiency of the "3-prong" case. And the red line shows the scenario if all decay modes were detected at the same efficiency as the "3-prong" case.

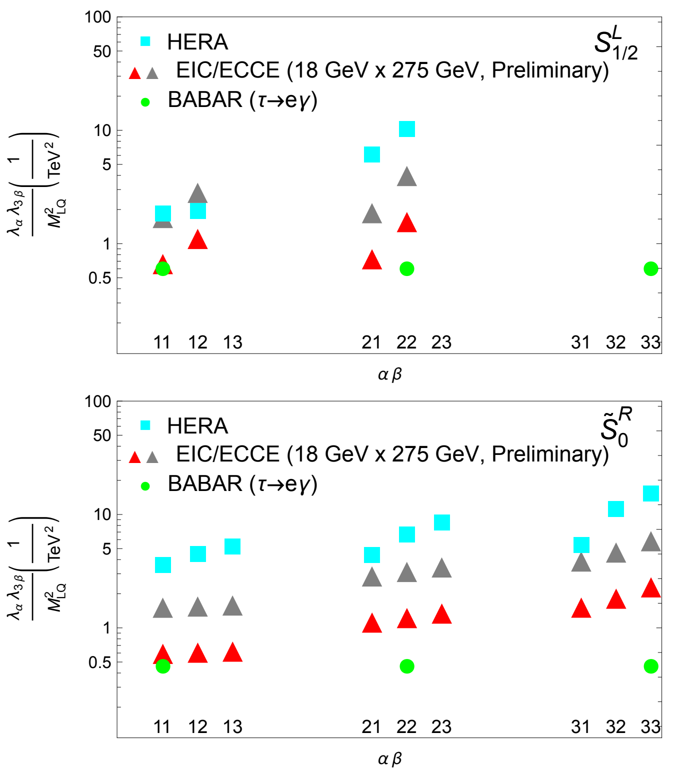

Figure 7: Limits on the scalar leptoquarks with $F = 0$ $S^L_{1/2}$ (top) and $|F| = 2$ $\tilde{S}^R_0$ (bottom) from 100 fb^{-1} of ep 18 × 275 GeV data, based on a sensitivity to leptoquark-mediated $ep \to \tau X$ cross section of size 1.7 fb (red triangles) or 11.4 fb (grey triangles) with ECCE. Note that due to small value of $\sqrt{s}$, EIC cannot constraint the third generation couplings of $S^L_{1/2}$ to top quarks. Limits from HERA [11, 5, 12, 6] are shown as cyan solid squares, and limits from $\tau \to e\gamma$ decays [3] are shown as green solid circles.

[5] S. Chekanov, et al., Search for lepton-flavor violation at HERA, Eur. Phys. J. C 44 (2005) 463–479. `arXiv:hep-ex/0501070`, `doi:10.1140/epjc/s2005-02399-1`.
[6] A. Aktas, et al., Search for lepton flavour violation in ep collisions at HERA, Eur. Phys. J. C 52 (2007) 833–847. `arXiv:hep-ex/0703004`, `doi:10.1140/epjc/s10052-007-0440-2`.
[7] B. Aubert, et al., Searches for Lepton Flavor Violation in the Decays tau+- —> e+- gamma and tau+- —> mu+- gamma, Phys. Rev. Lett. 104 (2010) 021802. `arXiv:0908.2381`, `doi:10.1103/PhysRevLett.104.021802`.
[8] M. Aaboud, et al., Search for lepton-flavor violation in different-flavor, high-mass final states in pp collisions at $\sqrt{s} = 13$ TeV with the ATLAS detector, Phys. Rev. D 98 (9) (2018) 092008. `arXiv:1807.06573`, `doi:10.1103/PhysRevD.98.092008`.
[9] E. D. P. A. Panel, Report from the EIC Detector Proposal Advisory Panel (2022).
URL `https://www.bnl.gov/dpapanelmeeting/files/pdf/dpap_report_3-21-2022_final.pdf`
[10] W. Buchmuller, R. Ruckl, D. Wyler, Leptoquarks in Lepton - Quark Collisions, Phys. Lett. B 191 (1987) 442–448, [Erratum: Phys.Lett.B 448, 320–320 (1999)]. `doi:10.1016/0370-2693(87)90637-X`.
[11] S. Chekanov, et al., Search for lepton flavor violation in e^+p col-

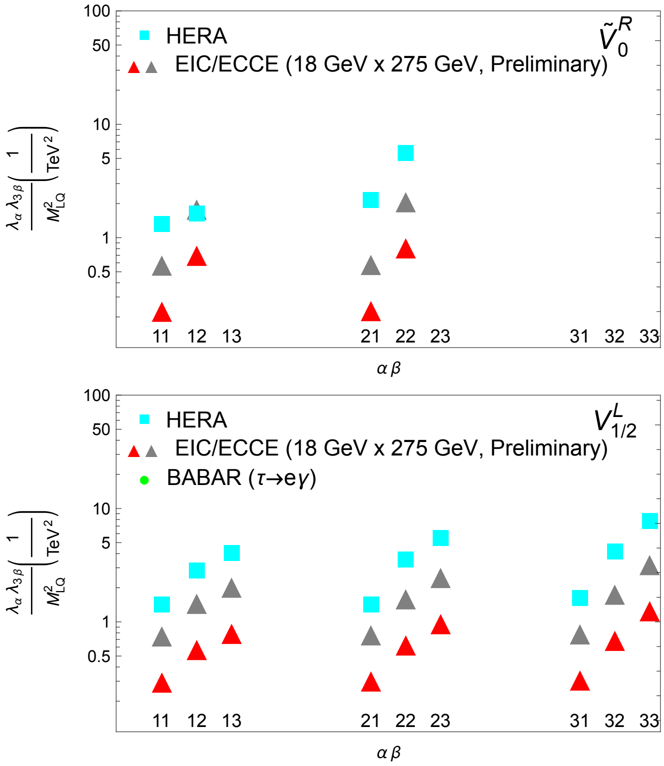

Figure 8: Limits on the vector leptoquarks with $F = 0$ $\tilde{V}_0^R$ (top) and $|F| = 2$ $V_{1/2}^L$ (bottom) from 100 fb^{-1} of ep 18×275 GeV data, based on a sensitivity to leptoquark-mediated $ep \to \tau X$ cross section of size 1.7 fb (red triangles) or 11.4 fb (grey triangles) from ECCE. Note that due to small value of $\sqrt{s}$, EIC cannot constraint the third generation couplings of $\tilde{V}_0^R$ to top quarks. Limits from HERA [11, 5, 12, 6] are shown as cyan solid squares. Limits from $\tau \to e\gamma$ decays [3] exist but require some work to convert to the 4-fermion contact term. This will be done in the future.

lisions at HERA, Phys. Rev. D 65 (2002) 092004. arXiv:hep-ex/0201003, doi:10.1103/PhysRevD.65.092004.

[12] C. Adloff, et al., A Search for leptoquark bosons and lepton flavor violation in e^+p collisions at HERA, Eur. Phys. J. C 11 (1999) 447–471, [Erratum: Eur.Phys.J.C 14, 553–554 (2000)]. arXiv:hep-ex/9907002, doi:10.1007/s100520050646.

[13] ECCE Consortium, EIC Comprehensive Chromodynamics Experiment Collaboration Detector Proposal, ecce-detector-proposal (2021).
URL https://www.ecce-eic.org/ecce-internal-notes

[14] A. Accardi, et al., Electron Ion Collider: The Next QCD Frontier: Understanding the glue that binds us all, Eur. Phys. J. A 52 (9) (2016) 268. arXiv:1212.1701, doi:10.1140/epja/i2016-16268-9.

[15] National Academies of Sciences, Engineering, and Medicine, An Assessment of U.S.-Based Electron-Ion Collider Science, The National Academies Press, Washington, DC, 2018. doi:10.17226/25171.
URL https://www.nap.edu/catalog/25171/an-assessment-of-us-based-electron-ion-collider-science

[16] L. Bellagamba, LQGENEP: A leptoquark generator for e p scattering, Comput. Phys. Commun. 141 (2001) 83–97. doi:10.1016/S0010-4655(01)00295-8.

[17] T. L. collaboration, Identification of beauty and charm quark jets at LHCb 10 (06) (2015) P06013–P06013. doi:10.1088/1748-0221/10/06/p06013.
URL https://doi.org/10.1088/1748-0221/10/06/p06013

Appendix A. Simulation Input Files and Other Details

Appendix A.1. LQGENEP Input Files for Leptoquark Signal Simulation

The input file for Leptoquark event generation using LQGENEP 1.0, for $Q^2_{\rm min} = 10$ GeV^2, is shown in Fig. A.9.

```
N_evt, Mass, MinQ2, beampar(2), beampar(3),  qi, qj, outfilename, seed
1000000, 1936.5, 10, 18, 275, 1, 1 LQGENEP_output_18x275_Qsq10_x0.001_1M_02.txt  3
```

Figure A.9: LQGENEP 1.0 input file for ep 18×275 GeV, $Q^2 > 10$ GeV^2 setting.

Appendix A.2. Djangoh Input Files for DIS NC and CC Background Event Simulation

DIS background NC and CC events were generated with Djangoh.4.6.10 , with the input files shown in Fig. A.10.

```
OUTFILENAM
erhic-cc-yrad-floff_ep_18_275_q2_1
TITLE
DJANGOH 4.6.10 for eRHIC for proton, NLO at 18x275, Wmin=1.4
EL-BEAM
        18.0D0    0.0D0    -1
IOUNITS
        6 10 11
PR-BEAM
        275.0D0   0.0D0
POLPDF
      0
GSW-PARAM
        2 1 3 1 1 1 1 2 1 1 1 1
KINEM-CUTS
        3   0.0000001D0  1.00D0  0.0000001D0  1.0D0  1.0D0  1D6  1.4D0
EGAM-MIN
        0D0
INT-OPT-NC
        0 0 0 0 0  0 0 0 0
INT-OPT-CC
        1 20 0 20
INT-ONLY
        0
INT-POINTS
        30000
SAM-OPT-NC
        0 0 0 0 0  0 0 0 0
SAM-OPT-CC
        1 1 0 1
NUCLEUS
        275.0D0  1   1
NUCL-MOD
        1000
STRUCTFUNC
        0  2  10150
LHAPATH
/u/group/eic/users/yxzhao/EW/lhapdf5/install/share
FLONG
        0  0.01  0.03
ALFAS
        1   1   0.20   0.235
NFLAVORS
        0   5
RNDM-SEEDS
        -1   1
START
        1000000
SOPHIA
        0
OUT-LEP
        1
FRAG
        1
CASCADES
        12
MAX-VIRT
        5
CONTINUE
```

```
OUTFILENAM
erhic-nc-yrad-floff_ep_18_275_q2_10
TITLE
DJANGOH 4.6.10 for eRHIC for proton, NLO at 18x275, Wmin=1.4
EL-BEAM
        18.0D0    0.0D0    -1
IOUNITS
        6 10 11
PR-BEAM
        275.0D0   0.0D0
POLPDF
      0
GSW-PARAM
        2 1 3 1 1 1 1 2 1 1 1 1
KINEM-CUTS
        3   0.0000001D0  1.00D0  0.0000001D0  1.0D0  1.0D1  1D6  1.4D0
EGAM-MIN
        0D0
INT-OPT-NC
        1 18 18 18 18  0 0 0 0
INT-OPT-CC
        0 0 0 0
INT-ONLY
        0
INT-POINTS
        30000
SAM-OPT-NC
        1 1 1 1 1  0 0 0 0
SAM-OPT-CC
        0 0 0 0
NUCLEUS
        275.0D0  1   1
NUCL-MOD
        1000
STRUCTFUNC
        0  2  10150
LHAPATH
/u/group/eic/users/yxzhao/EW/lhapdf5/install/share
FLONG
        0  0.01  0.03
ALFAS
        1   1   0.20   0.235
NFLAVORS
        0   5
RNDM-SEEDS
        -1   1
START
        1000000
SOPHIA
        3.4
OUT-LEP
        1
FRAG
        1
CASCADES
        12
MAX-VIRT
        5
CONTINUE
```

Figure A.10: Djangoh (4.6.10) input files for ep 18×275 GeV, DIS CC (left) and NC (right) background simulations for the leptoquark study. The $Q^2_{\rm min}$ is set at 1 GeV^2 and 10 GeV^2 for DIS CC and NC, respectively.

Appendix A.3. Pythia Input File for Photoproduction Background Simulation

The input file for photoproduction background generation using Pythia is shown in Fig. A.11.

```
pythia_ep_18x275_noradcor_Q2lt2.txt ! output file
name
11                ! lepton beam type
275, 18.0         ! proton and electron beam energy
2000000,100       ! Number of events
1e-09, 0.99       ! xmin and xmax
1e-09,1.00        ! ymin and ymax
1e-09,2           ! Q2min and Q2max
F2PY,1998         ! F2-Model, R-Parametrisation
0                 ! switch for rad corrections; 0:no, 1:yes,
2:gen.lookup table
1                 ! Pythia-Model = 0 standard GVMD
generation in Pythia-x and Q2; = 1 GVMD model with
generation in y and Q2 as for radgen
1,1               ! A-Tar and Z-Tar
1,1               ! nuclear pdf parameter1: nucleon mass number A,
charge number Z
201               ! nuclear pdf parameter2:
correction order x*100+y x= 1:LO, 2:NLO y:error set
! PMAS(4,1)=1.27    ! charm mass
MSEL=2
MSTP(14)=30
MSTP(15)=0
MSTP(16)=1
MSTP(17)=4 ! MSTP 17=6 is the R-rho measured as by
hermes, =4 Default
MSTP(18)=3
MSTP(19)=1 ! Hermes MSTP-19=1 different Q2
suppression, default = 4
MSTP(20)=0 ! Hermes MSTP(20)=0 , default MSTP(20)=3
MSTP(32)=8
MSTP(38)=4
MSTP(51)=7 ! if pdflib is linked than non pythia-
pdfs are available, like MSTP(51)=4046
MSTP(52)=1 ! ---> pdflib used MSTP   52=2
MSTP(53)=3
MSTP(54)=1
MSTP(55)=5
MSTP(56)=1
MSTP(57)=1
MSTP(58)=5
MSTP(59)=1
MSTP(60)=7
MSTP(61)=2
MSTP(71)=1
MSTP(81)=0
MSTP(82)=1
MSTP(91)=1
MSTP(92)=3      ! hermes MSTP(92)=4
MSTP(93)=1
MSTP(101)=3
MSTP(102)=1
MSTP(111)=1
MSTP(121)=0
! ------------- Now all the PARPs ---------------
PARP(13)=1
PARP(18)=0.40 ! hermes PARP(18)=0.17
PARP(81)=1.9
PARP(89)=1800
PARP(90)=0.16
PARP(91)=0.40
PARP(93)=5.
PARP(99)=0.40
PARP(100)=5
PARP(102)=0.28
PARP(103)=1.0
PARP(104)=0.8
PARP(111)=2.
PARP(161)=3.00
PARP(162)=24.6
PARP(163)=18.8
PARP(164)=11.5
PARP(165)=0.47679
PARP(166)=0.67597 ! PARP165/166 are linked to MSTP17 as R_rho of
HERMES is used
! PARP(166)=0.5
! ----------- Now come all the switches for Jetset -----------
PARJ(1)=0.100
PARJ(2)=0.300
PARJ(11)=0.5
PARJ(12)=0.6
PARJ(21)= 0.40
PARJ(32)=1.0
PARJ(33)= 0.80
PARJ(41)= 0.30
PARJ(42)= 0.58
PARJ(45)= 0.5
!-----------------------------------------------
MSTJ(1)=1
MSTJ(12)=1
MSTJ(45)=5
MSTU(16)=2
MSTU(112)=5
MSTU(113)=5
MSTU(114)=5
! ----------- Now all the CKINs for pythia ----------
CKIN(1)=1.
CKIN(2)=-1.
CKIN(3)=0.
CKIN(4)=-1.
CKIN(5)=1.00
CKIN(6)=1.00
CKIN(7)=-10.
CKIN(8)=10.
CKIN(9)=-40.
CKIN(10)=40.
CKIN(11)=-40.
CKIN(12)=40.
CKIN(13)=-40.
CKIN(14)=40.
CKIN(15)=-40.
CKIN(16)=40.
CKIN(17)=-1.
CKIN(18)=1.
CKIN(19)=-1.
CKIN(20)=1.
CKIN(21)=0.
CKIN(22)=1.
CKIN(23)=0.
CKIN(24)=1.
CKIN(25)=-1.
CKIN(26)=1.
CKIN(27)=-1.
CKIN(28)=1.
CKIN(31)=2.
CKIN(32)=-1.
CKIN(35)=0.
CKIN(36)=-1
CKIN(37)=0.
CKIN(38)=-1.
CKIN(39)=4.
CKIN(40)=-1.
CKIN(65)=1.e-09    ! Min for Q^2
CKIN(66)=-1.       ! Max for Q^2
CKIN(67)=0.
CKIN(68)=-1.
CKIN(77)=2.0
CKIN(78)=-1.
```

Figure A.11: Pythia (6.428) input files for photoproduction for *ep* 18×275 GeV setting.